IEEE Photonics Journal
An IEEE Photonics Society Publication

Invited Paper

Ultra-Wideband Radio-Over-Optical Fiber Concepts, Technologies and Applications

Volume 2, Number 1, February 2010

M. Ran
B. I. Lembrikov
Y. Ben Ezra

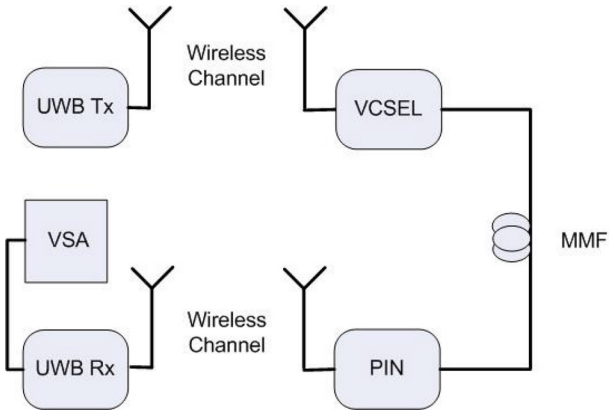

DOI: 10.1109/JPHOT.2010.2041055
1943-0655/$26.00 ©2010 IEEE

IEEE photonics SOCIETY formerly LEOS

IEEE

Ultra-Wideband Radio-Over-Optical Fiber Concepts, Technologies and Applications

M. Ran, B. I. Lembrikov, and Y. Ben Ezra

(Invited Paper)

Faculty of Engineering, Holon Institute of Technology, Holon 58102, Israel

DOI: 10.1109/JPHOT.2010.2041055

Manuscript received December 14, 2009. First published Online January 22, 2010. Current version published February 12, 2010. Corresponding author: B. I. Lembrikov (e-mail: borisle@hit.ac.il).

Abstract: We have developed novel ultra-wideband (UWB) radio-over-optical-fiber (UROOF) concepts and technologies for a number of important in-house applications characterized by a high data rate. We propose the novel components, architecture, and realization of UWB UROOF systems. We present new experimental results related to UWB signal up-conversion, photonic radio impulse generation, and digital and analog signal coexistence. We also discuss future trends in the field of UWB UROOF technologies.

Index Terms: Optical fiber communication, pulse generation, semiconductor laser, wireless local area network.

1. Introduction

The existing practical applications of short-range communication mainly takes the form of the Wireless Local Area Network (WLAN), the Wireless Personal Area Network (WPAN), and the Wireless Body Area Network (WBAN), which cover distances from tens of meters down to submeters [1]. New applications such as wireless multimedia and replacement of cables for communication purposes in home, office, and public access scenarios require an essential increase in data rates. In order to provide the higher data rates in future wireless systems, we should increase spectral efficiency (SE), design the systems with larger bandwidths, and reduce the costs per bit [1]. One of the most important candidate techniques for short-range communications that can satisfy these requirements is ultra-wideband (UWB) wireless communication [2]. UWB signals are characterized by an extremely large bandwidth. UWB frequency bands belong to 3.1–10.6 GHz according to the spectral mask defined by the Federal Communications Commission (FCC). WLAN and WPAN applications might be allowed to be deployed also across the frequency range of 57–66 GHz [3]. A very weak intensity comparable with the parasitic emission level is limited by a level of −41.3 dBm/MHz defined by the FCC, low complexity, high data rates, and localization and tracking features [2].

Modern UWB communication systems may be realized both in the impulse form and in multiband (MB) form [1]. In the case of the impulse radio (IR), information is carried in a set of narrow pulses of electromagnetic energy where the bandwidth is approximately proportional to the pulse width [1], [2]. In the MB case, the UWB spectrum is split into a number of subbands, which allows the use of narrowband techniques within each subband [1]. In particular, orthogonal frequency-division

multiplexing (OFDM) is a technique to transmit data in parallel by using a large number of modulated carriers with the subcarrier frequencies chosen in such a way that they are orthogonal over one OFDM symbol period [4]. Recently, OFDM has emerged as the leading physical-layer interface in broadband wireless communication systems due to a smaller intersymbol interference (ISI) caused by a dispersive channel and a transfer of the transmitters and receivers complexity from the analog to the digital domain [5], [6]. The MB UWB OFDM technology combines the advantages of SE data modulation formats (DMFs) and OFDM. However, UWB wireless technology applications are limited by short propagation distances of electromagnetic waveforms and multipath factors such as long delay and the difference between the output and the input signal [1]. For successful future applications, it is necessary to increase the data-transmission range at least up to 10–30 m [1].

Recently, we proposed a new concept that combines the advantages of the high-data-rate wireless short-range communications based on UWB technologies and, in particular, high SE and the optical fiber communication technology [2]. The proposed concept called UWB radio over fiber (UROOF) enables the transmission of UWB radio signals over optical fibers by superimposing the UWB radio frequency (RF) signals of several gigahertz on the optical continuous-wave (CW) carrier. It has the following advantages: 1) The bandwidth of the modulated carrier can reach a few percent of the carrier frequency providing the optical communication systems with the potential of carrying information at bit rates up to 1 Tb/s [7]; 2) the fiber losses are extremely low compared with other channel materials exhibiting a minimum loss of about 0.2 dB/km near the wavelength $\lambda = 1.55\ \mu$m [7]; 3) the conversion process becomes transparent to the UWB modulation method; 4) the high costs of additional electronic components required for synchronization and other processes can be avoided; 5) the integration of all the RF and optical transmitter/receiver components on a single chip is possible.

UROOF technology can significantly improve WPAN by range extension up to 2 to 3 orders of magnitude. Novel optical/wireless infrastructures can be developed to be capable of delivering broadband multimedia and above 1000-Mb/s traffic to subscribers in remote areas. UROOF technology can be used in security systems for collecting data from a large number of sensors and cameras equipped with UWB and transmitting it over optical infrastructures.

We used a UROOF transmission system consisting of a multimode fiber (MMF), directly modulated vertical cavity surface-emitting laser (VCSEL), and a photodetector (PD). In order to provide the highest possible bit rate, we developed different approaches to the optical/UWB conversion based on the heterojunction phototransistor (HPT), the optically controlled microwave convertor (OCMC), and the PIN diode. We investigated experimentally the UROOF transmission system performance in the case of the optical link and the combination of the optical link and wireless channel.

The paper is constructed as follows. The structure, components, and performance of the UROOF system are discussed in Section 2. The possibility of the UWB radio signals up-conversion from one frequency band group to another is discussed in Section 3. The IR UWB generation methods are presented in Section 4. The novel applications of the UROOF technologies are discussed in Section 5. Future trends of UROOF technologies are briefly reviewed in Section 6. Conclusions are presented in Section 7.

2. Ultra-Wideband Radio-Over-Optical-Fiber Transmission Channel

2.1. Optical Link

The fundamentals of UROOF technologies have been discussed in detail in [2]. The transmission line consisting of the optical link and wireless channel is shown in Fig. 1. The optical link consists of a transmitter, an optical fiber, and a PIN diode as PD, as shown in Fig. 1.

The VCSEL is characterized by low power consumption, high-speed modulation with low driving current, narrow circular beam for direct fiber coupling, low-cost and small-packaging capability, and single-longitudinal-mode operation with vertical microcavity [8]. The directly modulated VCSEL is

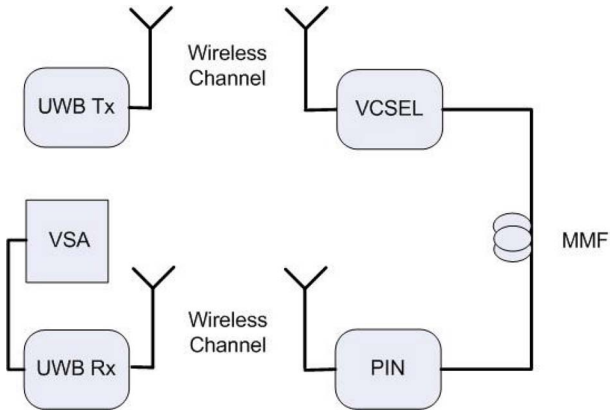

Fig. 1. Transmission line consisting of an optical link and a wireless channel.

described by the system of the rate equations for the photon density $P(t)$, electron density $N(t)$, and the phase $\phi(t)$ [7]

$$\frac{dP}{dt} = \left[\frac{\Gamma a(N - N_0)}{(1 + \varepsilon p)} - \alpha_{tot}\right] v_g P - \frac{P}{\tau_p} + \frac{\beta \Gamma N}{\tau_e} + F_P(t) \tag{1}$$

$$\frac{dN}{dt} = \frac{I(t)}{qV} - \frac{v_g a(N - N_0)}{(1 + \varepsilon p)} P - \frac{N}{\tau_e} - BN^2 - CN^3 + F_N(t) \tag{2}$$

$$\frac{d\phi}{dt} = \frac{1}{2}\alpha_c \left[\Gamma v_g a(N - N_0) - \frac{1}{\tau_p}\right] + F_\phi(t) \tag{3}$$

where a is the differential gain, N_0 is a transparency electron concentration, Γ is the confinement factor, v_g is the group velocity of light in the active region, V is the active region volume, $\tau_{p,e}$ are the photon and electron lifetimes, respectively, ε is the gain compression factor, β is the spontaneous emission fraction coupled into a lasing mode, q is the electron charge, $I(t)$ is the VCSEL bias current, B is the bimolecular recombination factor, C is the Auger recombination factor, α_c is the linewidth enhancement factor (LEF), α_{tot} is the total loss coefficient given by

$$\alpha_{tot} = \alpha_{loss} + \frac{1}{L}\ln\left(\frac{1}{R}\right) \tag{4}$$

where α_{loss} is the VCSEL absorption coefficient, L is the VCSEL active region length, and R is the reflectivity of the mirrors. The terms $F_P(t)$, $F_N(t)$, and $F_\phi(t)$ are the Langevin forces assumed to be Gaussian random processes. Single-mode rate equations (1)–(3) have been found to be a very good approximation of the large signal behavior for MMF [9].

The theoretical description of the VCSEL radiation modes propagating through MMF is based on the following assumptions [9]: 1) The transverse modes of a VCSEL are assumed to be Gaussian beam modes. 2) At the operating wavelength $\lambda = 850$ nm, the 50 μm, 1% Δ MMF initially supports 19 mode groups, each of which can have its own group velocity v_g. It is assumed that the coupling of modes within a mode group is significant over the short length scales of hundreds of meters, while the modal dispersion between mode groups is neglected. 3) The attenuation of the coupling modes within each group μ is described by the attenuation rate γ_μ, and the amplitude of a pulse launched into group μ is proportional to the factor $\exp(-\gamma_\mu z)$ as it propagates through MMF.

The analysis shows that the bandwidth and the MMF transfer function strongly depend on the excitation conditions that determine how much power will be coupled into each mode group, and the

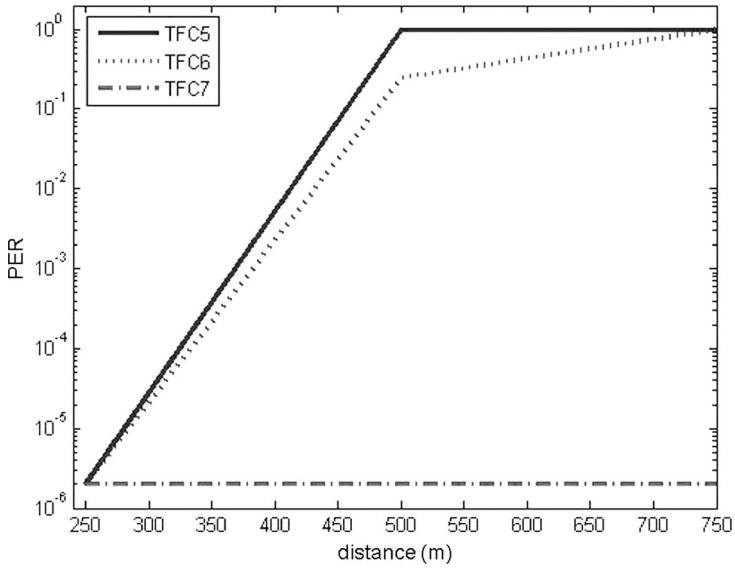

Fig. 2. PER dependence on the MMF length for TFC5, TFC6, and TFC7 frequency bands for the optical link.

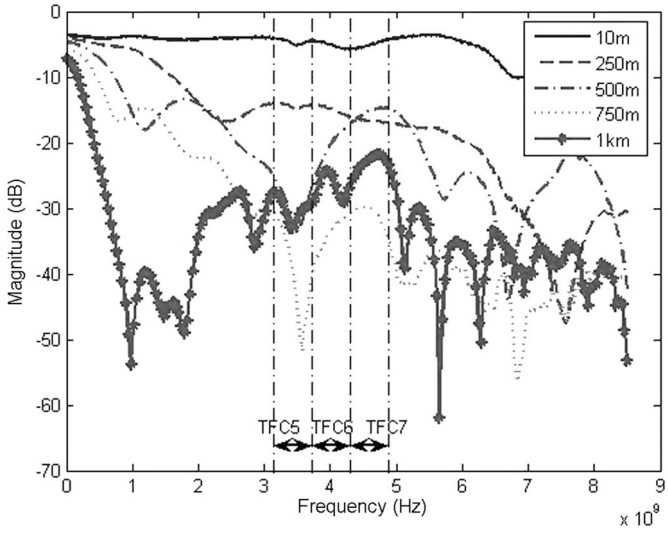

Fig. 3. Measurement results for the optical link frequency response.

signal at the receiver output is determined by the launch conditions, MMF properties, and the link configuration [9]. The impulse response of MMF $h(z, t)$ is given by [9]

$$h(z,t) = \sum_{\mu} w_{\mu} \exp(-\gamma_{\mu} z)\delta(t - \tau_{\mu} z) \tag{5}$$

where w_{μ} is the mode power distribution (MPD), and τ_{μ} is group delay per unit length.

A typical PIN PD is characterized by the quantum efficiency η and the bandwidth Δf given by [7], [10]

$$\eta = \frac{P_{abs}}{P_{opt}^{in}} = \zeta(1-r)(1-\exp(-\alpha_{PD} d)) \tag{6}$$

$$\Delta f = \left[\left(\frac{2\pi d}{3.5 \overline{v}_d} \right)^2 + \left(2\pi \varepsilon_0 \varepsilon_r S \frac{(R_s + R_l)}{d} \right)^2 \right]^{-1/2} \tag{7}$$

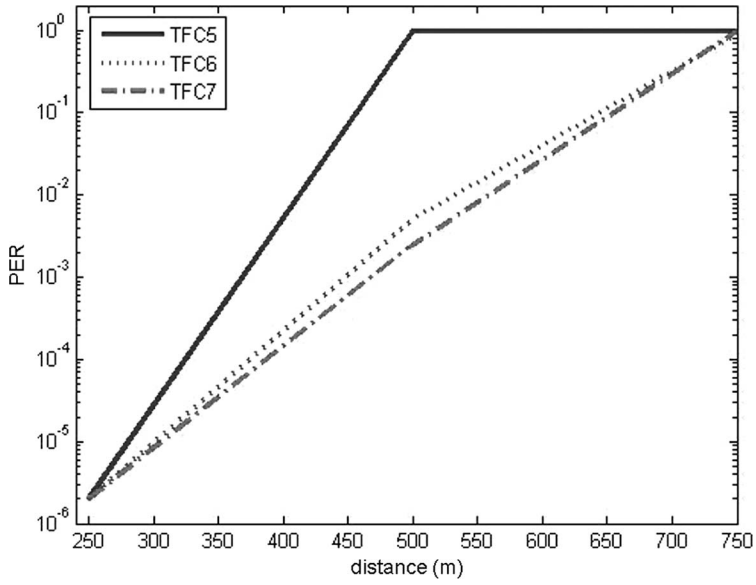

Fig. 4. PER dependence on the MMF length for the combined optical and wireless link.

where ζ is PIN PD internal quantum efficiency close to unity, P_{opt}^{in} is the incident optical power at the input of PD, P_{abs} is the optical power absorbed in PD, r is the reflection coefficient of the PD surface, α_{PD} is the PD material absorption coefficient, d is the thickness of the PD absorption intrinsic layer, $\overline{v}_d$ is the average charge carrier drift velocity in the PD absorption intrinsic layer, ε_0 is the free space permittivity, ε_r is the PD permittivity, S is the PD photosensitive area, and R_s, R_l are the series and load resistances in the PD equivalent circuit, respectively. The PIN PD bandwidth Δf is determined by the carrier transit time and RC time constant of the PIN PD equivalent circuit. The packet error rate (PER) dependence on the MMF length for the time frequency code 5 (TFC5), TFC6, and TFC7 bands measured for the optical link is shown in Fig. 2. The TFC5, TFC6, and TFC7 bands are determined by the frequency intervals (3168 ÷ 3696) MHz, (3696 ÷ 4224) MHz, and (4224 ÷ 4752) MHz, respectively. The measurement results for the optical link frequency response are shown in Fig. 3.

2.2. Wireless Link

Typically, the detected UWB signal should propagate from the transmitting antenna through a wireless channel. The UWB channel suffers from frequency-selective fading caused by large signal bandwidths exceeding the coherence bandwidth of the propagation environment [1]. In a UWB channel, there exists a large number of multipaths. The average total received energy is distributed between a number of multipath arrivals, and the amount of energy captured by a UWB receiving system increases until the number of multipath components is a few tens [1]. However, the delay caused by even a few tens components can be substantial [1]. The operation range is restricted by the low power spectral density [1].

The UWB wireless channel description is based on the modified Saleh–Valenzuela (SV) model [11]. In this model, the analytical representation of a discrete multipath impulse $h_i(t)$ can be presented as follows [11]:

$$h_i(t) = X_i \sum_{l=0}^{L_C^{-1}} \sum_{k=0}^{K_{LC}^{-1}} \alpha_{kl}^i \delta\left(t - T_l^i - \tau_{kl}^i\right) \tag{8}$$

where α_{kl}^i are the multipath gain coefficients, T_l^i are the delays of the lth cluster, and τ_{kl}^i is the delay for the kth multipath component relative to the lth cluster arrival time. Shadowing effect obeys the log-normal distribution and is represented by X_i, where i refers to the ith realization. The channel

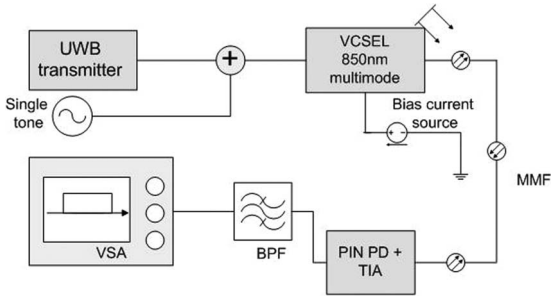

Fig. 5. Experimental setup for the triple-band up-conversion of OFDM UWB signals.

coefficients α_{kl} have the form $\alpha_{kl} = p_{kl}\xi_l\beta_{kl}$, where ξ_l is the fading associated with the lth cluster, and β_{kl} is the fading associated with the kth ray of the lth cluster [11].

The PER dependence on the MMF length for the combined optical and wireless link is shown in Fig. 4. A comparison of Figs. 2 and 4 shows a deterioration of the combined link performance for the TFC7 band.

3. Up-Conversion of Triple-Band Orthogonal Frequency Division Multiplexing Ultra-Wideband Signals by a Multimode Vertical Cavity Surface-Emitting Laser

Transmission of UWB radio signals over an optical fiber can provide a highly efficient solution for indoor networks since this technology overcomes the inherently short-range limitations that are typical for wireless channels [12], [13]. UWB based on MB OFDM is defined by [14], where the band groups 1, 2, and 3 belong to the frequency intervals of 3.168–4.224 GHz, 4.752–5.808 GHz, and 6.3336–7.362 GHz, respectively. MB OFDM technology can be implemented at the various parts of the spectral mask for UWB defined by the FCC, i.e., in the range of 3.1–10.6 GHz [15]. In order to comply with the requirements of different UWB regulations worldwide, it is sometimes necessary to up-convert UWB radio signals from frequency band group 1 to group 2 or 3. The up-conversion in question can be realized by electronic or optical methods. An efficient and low-cost optical microwave (MW) mixer can provide a flexible solution for a transition between different MB OFDM signals. Such a mixer can be used in order to shift MB OFDM signals available at the American UWB band of about 5–6 GHz to higher frequency European and Japanese UWB bands. In particular, the applications based on the UROOF technology combine the up-conversion with the nonlinear mixing of optical signals generated by an MM VCSEL. MM 850-nm VCSELs are characterized by a high bandwidth and low cost. However, in order to benefit from these VCSEL advantages, it is necessary to use MMF as the optical link. The MMFs are also attractive because they are already installed in many large buildings. Recently, a low-cost optical mixer based on the VCSEL nonlinearity has been reported [16]. The up-conversion by a frequency of 2.1 GHz has been carried out using a 1550-nm VCSEL [16].

We have carried out, for the first time, the low-cost and high-performance method for the up-conversion of the triple-band OFDM UWB signals based on the nonlinear properties of the MM 850-nm VCSEL [17]. We evaluated experimentally the efficiency of the second- and third-order intermodulations as a function of the bias current and signal and local oscillator power level. In order to characterize the up-conversion performance, we have measured the error vector magnitude (EVM). We have also measured the spectra of the second- and third-order intermodulation products. For the first time, according to our best knowledge, we have demonstrated the feasibility of the converting of the UWB signals belonging to the frequency band group 1 up to the required frequency band groups 2 and 3 [17]. The experimental setup is shown in Fig. 5.

In our experiments, we have used a Finisar MM VCSEL of a 850-nm wavelength biased by a stabilized HP E3620A current source. A Wisair UWB transmitter provided the MB OFDM signals with a central frequency of 3.432 GHz and bandwidth of 5.28 GHz. The UWB power has been kept

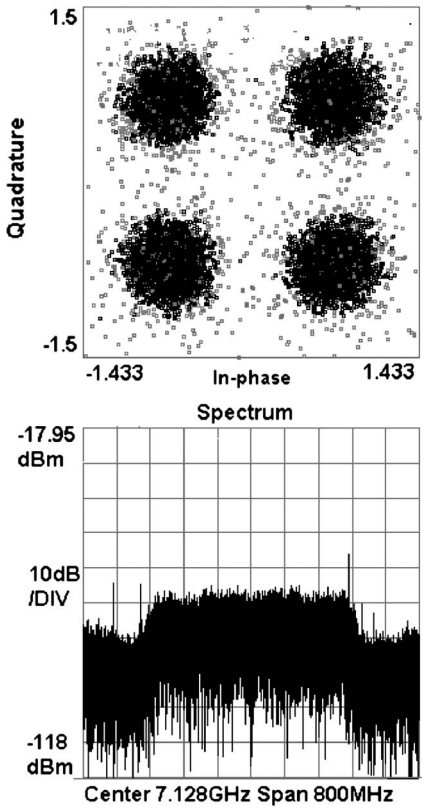

Fig. 6. Spectrum and constellation diagram of the transmitted signal.

at the level of -14 dBm according to the FCC. The MB OFDM signal was combined with a CW signal of the local oscillator (LO) Agilent E8257C of the frequency 2 GHz $\leq f_{LO} \leq$ 6 GHz and fed into the MM VCSEL as a the modulating signal. The VCSEL output has been detected by using a Finisar PIN PD, transmitted through a 3-m MMF link and amplified by a transimpedance amplifier.

The triple-band UWB OFDM signal consisting of the time frequency code 5 (TFC5), TFC6, and TFC7 bands was converted to the optical domain by using of MM VCSEL, transmitted through MMF, and detected by a PIN diode according to the experimental setup shown in Fig. 5. The UWB OFDM signal power is $P_{UWB} = -14$ dBm, and each band containing 128 subcarriers carries information at a bit rate of 480 Mb/s. The constellation and spectrum of the detected triple band are shown in Fig. 6.

The nonlinear mixing efficiency is evaluated by measuring the conversion loss of the corresponding intermodulation signal essentially determined by the nonlinearity of the VCSEL's emitted optical power dependence on the bias current. The second-order intermodulation conversion loss as a function of the bias current for different LO power levels is shown in Fig. 7.

The conversion loss is in the range of 20–25 dB and has a minimum at the optimal bias current of about 2 mA, which is close to the VCSEL threshold current where the second-order nonlinearity is especially strong. The quality of the up-converted UWB OFDM signal passing through the whole link is determined by the second-order intermodulation EVM degradation ΔEVM. The ΔEVM dependence on the VCSEL bias current shown in Fig. 8 clearly manifests that ΔEVM reaches its minimum at the same bias current as the conversion loss minimum occurs.

In our case, the intermodulations with the up-converted sum frequency $f_{UWB} + f_{LO}$ of UWB central carrier and LO signal and the LO second harmonic $2f_{LO}$ appeared to be very close. Due to the large bandwidth of UWB OFDM signal, its spectrum involves the sum frequency $f_{UWB} + f_{LO}$, which

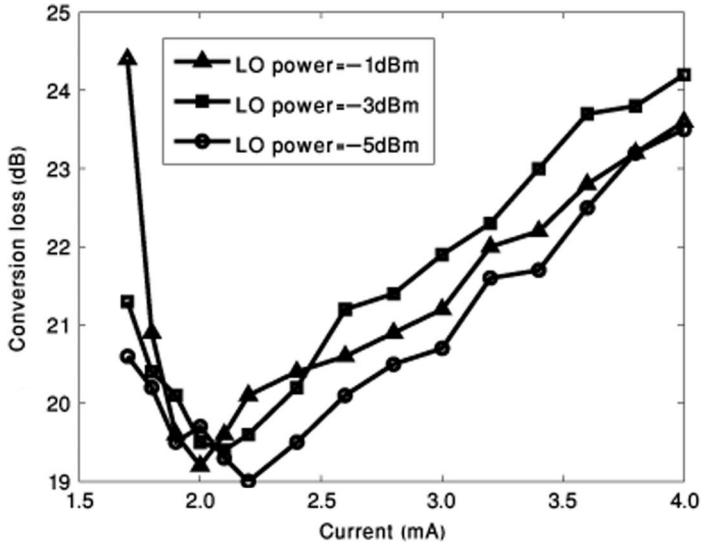

Fig. 7. Second-order intermodulation EVM degradation dependence on the VCSEL bias current for different LO signal power levels.

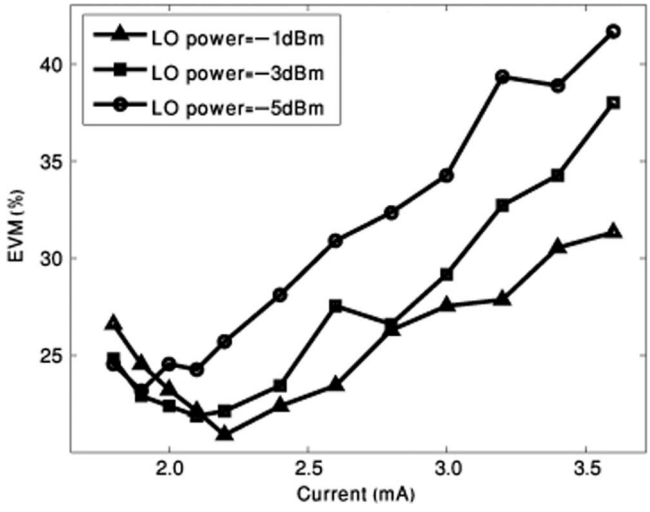

Fig. 8. Second-order intermodulation EVM degradation dependence on the VCSEL bias current for different LO signal power levels.

consequently cannot be singled out. This bandwidth overlapping limits the possibility of the up-conversion for a wide range of the UWB OFDM signal frequencies.

For this reason, we have also carried out the UWB OFDM signal up-conversion by means of the third-order intermodulation. The conversion losses dependence on the VCSEL bias current for three different UWB OFDM signal frequencies are shown in Fig. 9. This time, the conversion loss has the minimum value at the bias current of about 3 mA and remains low and approximately constant at larger bias currents up to 7 mA. These current values correspond to the interval in the vicinity of the inflexion point of the VCSEL power-bias current curve where the third-order VCSEL nonlinearity is essential. Typically, in the case of the third-order nonlinearity, the distortion terms of the type $2f_{UWB} + f_{LO}$ and $2f_{LO} + f_{UWB}$ fall outside the UWB OFDM signal bandwidth, which makes it possible the up-conversion of a wide range of frequencies. The UWB OFDM signal up-conversion

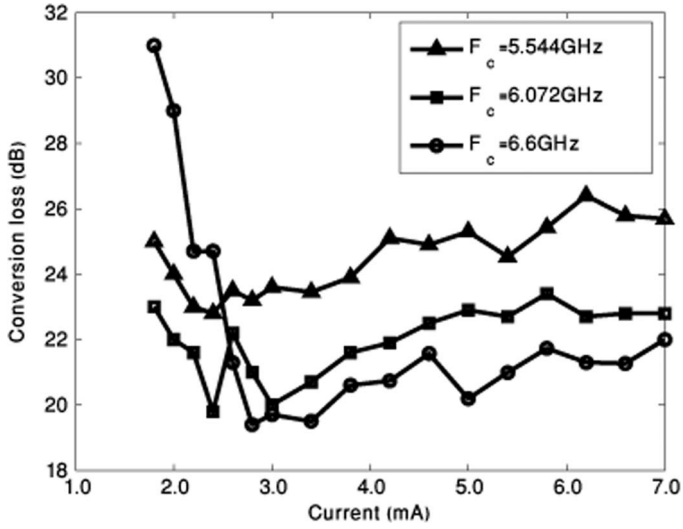

Fig. 9. Third intermodulation conversion loss dependence on the VCSEL bias current.

based on the third-order VCSEL nonlinearity is more efficient as compared with the second-order nonlinearity case.

4. Optical Techniques of Impulse Radio Ultra-Wideband Generation

The IR UWB communication technique is carrier free and uses, for communication between transmitters and receivers, very narrow RF pulses generated from the UWB pulse generator, while traditional transmission systems transmit information by varying the power, frequency, and/or phase of a sinusoidal wave in a modulation process [18], [19]. The selection of the impulse signal type for IR UWB communication system is essential since it determines the system performance [19]. Gaussian pulses are the most widely used waveforms due to their simplicity and achievability [19]. Previously, most of the approaches to generating of IR UWB signals were based on electronic methods [20]. Recently, optically based methods of the IR-UWB pulse signal generation for low-cost high-data-rate UWB wireless systems have attracted a great deal of interest due to the decreasing of interference between electrical devices, low loss, and light weight of optical fibers [20], [21]. A number of such schemes for the generation of Gaussian IR-UWB monocycles and doublets [13] has been proposed [21]–[26]. Typically, an optically based system generating Gaussian IR-UWB monocycles and doublets consists of an electrooptic phase modulator (EOM), a single-mode fiber (SMF), an Erbium-doped fiber amplifier (EDFA), a fiber Bragg grating (FBG), and a PD [20]–[23].

We proposed a new all-optical approach to the UWB pulse signal generation based on cross phase modulation (XPM) and cross-gain modulation (XGM) in quantum-dot semiconductor optical amplifiers (QD SOAs) [27]. A QD SOA is characterized by an extremely high optical nonlinearity and high operation rate [28]–[31], especially as compared with EDFA [7]. We used the nonlinear properties of a Mach–Zehnder interferometer (MZI) with an active element [32]. In a proposed method, a QD SOA as a nonlinear element is inserted into one arm of the integrated MZI, which results in an intensity-dependent optical signal interference at the output of MZI. The theoretical analysis of the nonlinear MZI containing QD SOA based on the QD SOA dynamics and truncated equations for optical pulses propagation clearly shows that the proposed method permits generation of UWB-IR monocycle pulses with an adjustable duration in the range of picoseconds. Moreover, QD SOA based MZI structure is an integrable and concise component of all-optical communication systems.

The block diagram of the proposed all-optical UWB-IR pulse generator consisting of a CW laser, a pulse laser, and an MZI with a QD SOA in its upper arm is shown in Fig. 10.

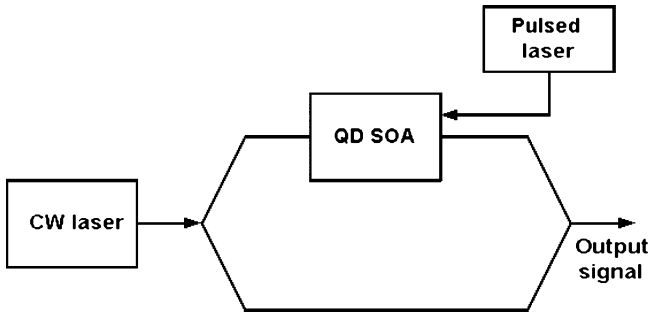

Fig. 10. Block diagram of the proposed UWB-IR generator.

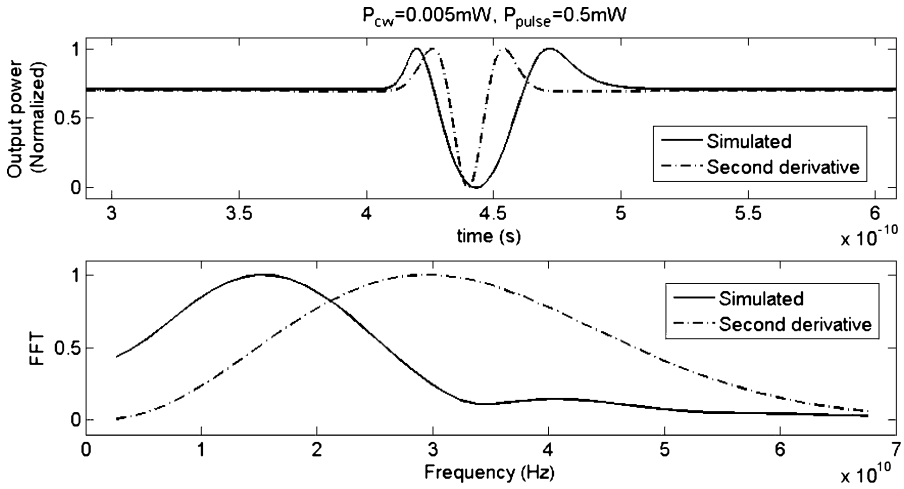

Fig. 11. (Top) (Solid line) Gaussian doublet and (dashed line) the second derivative of the standard Gaussian pulse. (Bottom) (Solid line) Fast Fourier transforms (FFT) of the simulated IR-UWB pulse and (dashed line) the second derivative of the standard Gaussian pulse.

A CW beam of a wavelength λ and an optical power P_0 is split into two equal optical power beams and fed into the two ports of the integrated MZI, one of which contains a QD SOA. The pulse laser produces a train of short Gaussian pulses counter-propagating with respect to the input CW optical signal. The CW signal propagating through the upper arm of the MZI transforms into the Gaussian beam at the output of the MZI due to XPM and XGM with the train of Gaussian pulses whereas the beam in the linear lower arm of MZI remains CW. Both these beams interfere at the output of MZI, and the output beam shape is defined by the power dependent phase difference.

The system of dynamics and propagation equations for QD-SOA and MZI has been solved numerically for the typical values of the QD SOA parameters [33]–[35]. The simulation results for the Gaussian doublet and its spectrum are shown in Fig. 11. The simulation results clearly show that UWB signals generated by the proposed QD SOA-based MZI structure comply with the FCC definitions of UWB-IR signals.

An alternative method of all-optical generation of UWB Gaussian monocycles and doublets is based on the system of two integrated unbalanced MZIs (UMZIs) connected in parallel or in cascade that contain no active elements [36]. The UMZIs are chosen in such a way that the phase difference of the interfering signals at the output is equal to π. Each one of the UMZIs is characterized by time delay differences τ and 2τ. As a result, at the output of the UMZIs the interfering optical signals UWB modulated by a Gaussian UWB pulse form the first-order difference approximating the Gaussian monocycle and the second-order difference approximating the Gaussian doublet. At the output of the system, the UWB monocycles and doublets can be converted to a UWB signal by means of a homodyne detection where the local oscillator frequency

ω_{LO} coincides with the optical carrier frequency ω [7]. In such a case, the detected signal is proportional to the UWB modulated optical signal amplitude [7], i.e., to the Gaussian monocycle or doublet in our case. The system can be made tunable by including into the UMZIs a tunable delay line. The proposed scheme can also be used for all-optical signal denoising [36].

5. Applications of Ultra-Wideband Technologies

Several novel UROOF system application scenarios are reviewed below.

1. **WPAN range extension**. Inherently, the high-data-rate UWB signals are available today only for short-range distances of less than 10 m. The range extension over a hybrid fiber-wireless channel based on low-cost UROOF technologies enables the extension of this by two orders of magnitude. The UWB range-extension application overall performance depends on the number of simultaneous users, the traffic, and the modulation type (given the packet length) used.
2. **Very low-cost distributed antenna system (VL-DAS)**. Several access points equipped with UROOF transceivers, each located in different femto-net locations, are connected through radio-over-fiber (RoF) links to a central station. UWB signals are passing over the wireless/RoF channel among the access points. Potentially, VL-DAS architectures based on UROOF can support the needs of 1 Gb/s fourth-generation technology.
3. **Security and home land applications**. A collection of UROOF nodes (e.g., sensor networks) capable of transmitting simultaneously through radio-UWB and RoF are all connected to a control station via optical, enabling low-latency, location-enabled, and secure (by beamforming) communications.
4. **Capacity expansion of Hybrid Coax (HFC) systems**. This approach aims to achieve 100–480 Mb/s over existing HFC infrastructure by superimposing a UWB signal into existing data signals. Properly precompensated UWB signals are capable of coexisting with the currently deployed HFC spectrum or even with the actual dc- to 3-GHz spectrum of the coax.
5. **Intelligent transportation systems (ITS)**. Road-to-vehicle and vehicle-to-vehicle are the basic components of evolving technologies to increase safety on roads and enable a comfortable mobile traffic environment. Recently, a new family of IEEE standards aimed at providing communications between cars and roadside infrastructure has been approved for trial use. This family, which is known as the IEEE 1609 suit of Wireless Access in Vehicular Environments (WAVE), is based on existing 802.11 short-range communications at 5.9 GHz. UROOF technologies can be integrated into the ITS concept and provide means to adding broadcasting and anti-collision radar information.

6. Ultra-Wideband Technology Prospectives

We believe that some novel aspects of UROOF technologies, such as architecture of UWB OFDM systems, UWB transmission in the 60-GHz frequency band, and novel ultra-fast photonic components, are important for further research. Parallel and serial architectures of UWB OFDM systems should be explored in order to construct multiband OFDM signals capable of delivering a multigigabit analog signal. We address beyond 40-Gb/s data rates by parallel transmission over more than 128 conventional baseband channels, each having 528-MHz bandwidth. The parallel RF/serial optic architecture enables various operations with channels and bands. In the alternative scheme of the parallel RF/parallel optics architecture, each directly modulated low-cost MM VCSEL with a 10-Gb/s bandwidth transmits its signal over a separate MMF. In contrast to the parallel RF/serial optics architecture, with SMF suitable for long-haul applications, this version based on MMF is appropriate for short-range applications.

A 57–64-GHz channel mentioned above may be especially useful for future WPAN applications. Recently, 60-GHz MB OFDM up-conversion in the UROOF system has been demonstrated [37], [38].

In UROOF technology, detection of the multiplexed MB OFDM UWB modulated optical signal is required. The down conversion from the optical domain to the UWB or MW domain can be modeled

by an optically controlled load connected at the open end of a microstrip (MS) line. The SiGe/Si structures are promising candidates for high-speed optoelectronics receivers due to the high operation rate, comparatively optical high absorption coefficient, the possibility of operation in the near-infrared spectrum from 850 nm to 1550 nm, and low noise and compatibility with Si-based electronic components. Recently, we proposed an analytical model of the thin-layer SiGe/Si OCMC structure with a detecting layer thickness of about $d = (0.5 \div 2)\ \mu$m [39]. The numerical estimations based on this model show that a bandwidth of at least 20 GHz can be achieved [39].

Multiple-input multiple-output (MIMO) OFDM is a promising candidate technique for short-range communications [1]. The combination of the optical MIMO and MB-OFDM over MM fiber further extends the performance of UROOF. Broadband MIMO systems provide higher capacity, higher link reliability, and better quality of service, similar to a wire channel [1].

Recent developments in quantum dot (QD) lasers grown directly on Si and their on-chip integration with Si waveguides, electroabsorption modulators, and detectors provide the possibility of the monolithic integration of Si photonics and electronics on an Si platform [40]. Such a system is characterized by an ultralow power dissipation, low bias current, a very high temperature stability, and exceptionally high bandwidth [40]. Optoelectronic devices based on Integrated QD lasers and Si photonic components are promising candidates for a future generation of ultra-fast, low-power UWB systems.

7. Conclusion

We discussed in detail the structure, theoretical models, and performance characteristics of a UROOF system. We presented novel original experimental and simulation results concerning the proposed UROOF system performance, UWB frequency up-conversion, and photonic IR-UWB generation. We have also briefly reviewed some applications and novel promising trends in UWB technologies and their components.

References

[1] G. Fettweis, E. Zimmermann, B. Allen, D. C. O'Brien, and P. Chevillat, "Short-range wireless communications," in *Technologies for the Wireless Future*, R. Tafazolli, Ed. New York: Wiley, 2006.

[2] M. Ran, Y. Ben Ezra, and B. Lembrikov, "Ultra-wideband radio-over-optical fibre," in *Short-Range Wireless Communications: Emerging Technologies and Applications*, R. Kraemer and M. Katz, Eds. New York: Wiley, 2009, Part IV: Emerging Concepts in Short-Range Communications, ch. 24, pp. 271–327.

[3] I. Siaud, A.-M. Ulmer-Moll, N. Malhouroux-Gaffet, and G. Valery, "An introduction to 60 GHz communication systems: Regulation and services, channel propagation and advanced baseband algorithms," in *Short-Range Wireless Communications: Emerging Technologies and Applications*, R. Kraemer and M. Katz, Eds. New York: Wiley, 2009, Part III: 60 GHz Communication Systems: Concepts and Implementation Aspects.

[4] L. W. Couch, II, *Digital and Analog Communication Systems*. Upper Saddle River, NJ: Prentice-Hall, 2001.

[5] W. Shieh, H. Bao, and Y. Tang, "Coherent optical OFDM: Theory and design," *Opt. Express*, vol. 16, no. 2, pp. 841–859, Jan. 2008.

[6] J. Armstrong, "OFDM for optical communications," *J. Lightw. Technol.*, vol. 27, no. 3, pp. 189–204, Feb. 2009.

[7] G. P. Agrawal, *Fiber-Optic Communication Systems*. New York: Wiley, 2002.

[8] F. Koyama, "Recent advances of VCSEL photonics," *J. Lightw. Technol.*, vol. 24, no. 12, pp. 4502–4513, Dec. 2006.

[9] P. Pepeljugoski, S. E. Golowich, A. J. Ritger, P. Kolesar, and A. Risteski, "Modeling and simulation of next-generation multimode fiber links," *J. Lightw. Technol.*, vol. 21, no. 5, pp. 1242–1255, May 2003.

[10] S. Malyshev and A. Chizh, "State of the art high-speed photodetectors for microwave photonics applications," in *Proc. 15th Int. Conf. MIKON*, Warsaw, Poland, May 17–19, 2004, vol. 3, pp. 765–775.

[11] M. Hämäläinen, V. Hovinen, and L. Hentilä, "UWB channel models," in *UWB Theory and Applications*, I. Oppermann, H. Hämäläinen, and J. Linatti, Eds. Chichester, U.K.: Wiley, 2004, pp. 9–38.

[12] I. Oppermann, "The role of UWB in 4G," *Wireless Pers. Commun.*, vol. 29, no. 1/2, pp. 121–133, Apr. 2004.

[13] M. Ghavami, L. B. Michael, and R. Kohno, *Ultra Wideband Signals and Systems in Communication Engineering*. Chichester, U.K.: Wiley, 2005.

[14] *High Rate Ultra Wideband PHY and MAC Standard*, ECMA-368, Dec. 2005, 1st ed.

[15] Federal Communications Commission (FCC), Rules and Regulations. [Online]. Available: http://www.fcc.gov/searchtools.html

[16] S. B. Constant, Y. Le Guennec, G. Maury, N. Corrao, and B. Cabon, "Low-cost all-optical up-conversion of digital radio signals using a directly modulated 1550-nm emitting VCSEL," *IEEE Photon. Technol. Lett.*, vol. 20, no. 2, pp. 120–122, Jan. 2008.

[17] Y. Ben Ezra, M. Ran, B. I. Lembrikov, B. Cabon, A. Leibowitch, and M. Haridim, "Up-conversion of triple-band OFDM UWB signals by a multimode VCSEL," *IEEE Photon. Technol. Lett.*, vol. 21, no. 13, pp. 869–871, Jul. 2009.

[18] R. S. Kshetrimayum, "An introduction to UWB communication systems," *IEEE Potentials*, vol. 28, no. 2, pp. 9–13, Mar./Apr. 2009.
[19] J. Yao, F. Zeng, and Q. Wang, "Photonic generation of ultrawideband signals," *J. Lightw. Technol.*, vol. 25, no. 11, pp. 3219–3235, Nov. 2007.
[20] Q. Wang and J. Yao, "UWB doublet generation using nonlinearly-biased electro-optic intensity modulator," *Electron. Lett.*, vol. 42, no. 22, pp. 1304–1305, Oct. 2006.
[21] W.-P. Lin and J.-Y. Chen, "Implementation of a new ultrawide-band impulse system," *IEEE Photon. Technol. Lett.*, vol. 17, no. 11, pp. 2418–2420, Nov. 2005.
[22] F. Zeng and J. Yao, "An approach to ultrawideband pulse generation and distribution over optical fiber," *IEEE Photon. Technol. Lett.*, vol. 18, no. 7, pp. 823–825, Apr. 2006.
[23] F. Zeng and J. Yao, "Ultrawideband impulse radio signal generation using a high-speed electrooptic phase modulator and a fiber-Bragg-grating-based frequency discriminator," *IEEE Photon. Technol. Lett.*, vol. 18, no. 19, pp. 2062–2064, Oct. 2006.
[24] Y. Le Guennec, G. Maury, J. Yao, and B. Cabon, "New optical microwave up-conversion solution in radio-over-fiber networks for 60-GHz wireless applications," *J. Lightw. Technol.*, vol. 24, no. 3, pp. 1277–1282, Mar. 2006.
[25] Y. Le Guennec and R. Gary, "Optical frequency conversion for millimeter-wave ultra-wideband-over-fiber systems," *IEEE Photon. Technol. Lett.*, vol. 19, no. 13, pp. 996–998, Jul. 2007.
[26] F. Zeng, O. Wang, and J. P. Yao, "All-optical UWB impulse generation based on cross-phase modulation and frequency discrimination," *Electron. Lett.*, vol. 43, no. 2, pp. 119–121, Jan. 2007.
[27] Y. Ben Ezra, M. Haridim, B. I. Lembrikov, and M. Ran, "Proposal for all-optical generation of ultra wideband impulse radio signals in Mach–Zehnder interferometer with quantum dot optical amplifier," *IEEE Photon. Technol. Lett.*, vol. 20, no. 7, pp. 484–486, Apr. 2008.
[28] M. Sugawara, H. Ebe, N. Hatori, M. Ishida, Y. Arakawa, T. Akiyama, K. Otsubo, and Y. Nakata, "Theory of optical signal amplification and processing by quantum-dot semiconductor optical amplifiers," *Phys. Rev. B, Condens. Matter*, vol. 69, no. 23, pp. 235332-1–235332-39, Jun. 2004.
[29] N. N. Ledentsov, "Long-wavelength quantum-dot lasers on GaAs substrates: From media to device concepts," *IEEE J. Sel. Topics Quantum Electron.*, vol. 8, no. 5, pp. 1015–1024, Sep./Oct. 2002.
[30] A. V. Uskov, T. W. Berg, and J. Mørk, "Theory of pulse-train amplification without patterning effects in QD semiconductor optical amplifiers," *IEEE J. Quantum Electron.*, vol. 40, no. 3, pp. 306–320, Mar. 2004.
[31] T. W. Berg, J. Mørk, and J. M. Hvam, "Gain dynamics in semiconductor quantum dot amplifiers," *New J. Phys.*, vol. 6, pp. 178–200, 2004.
[32] G. P. Agrawal, *Applications of Nonlinear Fiber Optics*. New York: Academic, 2001.
[33] Y. Ben-Ezra, M. Haridim, and B. I. Lembrikov, "Theoretical analysis of gain-recovery time and chirp in QD-SOA," *IEEE Photon. Technol. Lett.*, vol. 17, no. 9, pp. 1803–1805, Sep. 2005.
[34] Y. Ben-Ezra, B. I. Lembrikov, and M. Haridim, "Acceleration of gain recovery and dynamics of electrons in QD-SOA," *IEEE J. Quantum Electron.*, vol. 41, no. 10, pp. 1268–1273, Oct. 2005.
[35] Y. Ben-Ezra, B. I. Lembrikov, and M. Haridim, "Specific features of XGM in QD-SOA," *IEEE J. Quantum Electron.*, vol. 43, no. 8, pp. 730–737, Aug. 2007.
[36] Y. Ben-Ezra and B. I. Lembrikov, "Optical wavelet signal processing," in *Proc. 11th Int. Conf. Transparent Opt. Netw.*, Azores, Portugal, Jun. 28–Jul. 2, 2009, pp. 1–4, *(Invited Paper)*, We. A.2.2.
[37] R. Gary, B. Cabon, and Y. Le Guennec, "60 GHz UWB over fiber system using photodiode-based frequency up-conversion," *Microw. Opt. Technol. Lett.*, vol. 51, no. 2, pp. 421–423, Feb. 2009.
[38] G. H. Nguyen, B. Cabon, and Y. Le Guennec, "Generation of 60 GHz MB-OFDM signal-over-fiber by up-conversion using cascaded external modulators," *J. Lightw. Technol.*, vol. 27, no. 11, pp. 1496–1502, Jun. 2009.
[39] B. I. Lembrikov and Y. Ben Ezra, "The possibility of UWB signal detection in a thin SiGe layer," in *Proc. Eur. Workshop Photon. Solutions Wireless Access In-House Netw.*, Duisburg, Germany, May 18–20, 2009, pp. 73–74.
[40] Z. Mi, J. Yang, P. Bhattacharya, G. Qin, and Z. Ma, "High-performance quantum dot lasers and integrated optoelectronics on Si," *Proc. IEEE*, vol. 97, no. 7, pp. 1239–1249, Jul. 2009.